Inorg. Chem. **2008**, *47*, 2074−2082

A Family of Cyanide-Bridged Molecular Squares: Structural and Magnetic Properties of $[\{M^{II}Cl_2\}_2\{Co^{II}(triphos)(CN)_2\}_2]\cdot xCH_2Cl_2$, M = Mn, Fe, Co, Ni, Zn

Ferdi Karadas,[†] Eric J. Schelter,[†] Michael Shatruk,[†,||] Andrey V. Prosvirin,[†] John Bacsa,[†] Dmitry Smirnov,[‡] Andrew Ozarowski,[‡] J. Krzystek,[‡] Joshua Telser,[§] and Kim R. Dunbar*[,†]

Department of Chemistry, Texas A&M University, P.O. Box 30012, College Station, Texas 77842-3012, National High Magnetic Field Laboratory, Florida State University, 1800 E. Paul Dirac Dr., Tallahassee, Florida 32310, and Department of Biological, Chemical and Physical Sciences, Roosevelt University, Chicago, Illinois 60605

Received October 22, 2007

The syntheses, structures, and magnetic properties of a series of tetranuclear cyanide-bridged compounds are reported. This family of molecular squares, $[\{M^{II}Cl_2\}_2\{Co^{II}(triphos)(CN)_2\}_2]$ (M = Mn (**[CoMn]**), Fe (**[CoFe]**), Co (**[CoCo]**), Ni (**[CoNi]**), and Zn (**[CoZn]**), triphos = 1,1,1-tris(diphenylphosphinomethyl)ethane), has been synthesized by the reaction of $Co^{II}(triphos)(CN)_2$ and MCl_2 (M = Mn, Co, Ni, Zn) or $Fe_4Cl_8(THF)_6$ in a CH_2Cl_2/EtOH mixture. These complexes are isostructural and consist of two pentacoordinate Co(II) and two tetrahedral M(II) centers. The resulting molecular squares are characterized by antiferromagnetic coupling between metal centers that generally follows the spin-coupling model $S_{total} = S_{M(II)1} - S_{Co1} + S_{M(II)2} - S_{Co2}$. Magnetic parameters for all the complexes were measured using SQUID magnetometry. Additionally, **[CoZn]** and **[CoMn]** were studied by both conventional and high-frequency and high-field electron paramagnetic resonance.

Introduction

Polynuclear metal complexes are widely studied due to their fascinating catalytic, photophysical, electronic, and magnetic properties.[1] Among these complexes, molecular squares represent one of the simplest types of molecular architectures. Because of their structural simplicity, the physical properties of molecular squares can often be interpreted, provided that one is armed with a basic knowledge of the behavior of the parent mononuclear building blocks. Research in our group and in other laboratories has focused on the chemistry of magnetic molecular squares that form readily under thermodynamic control with a careful choice of ML_n precursors.[2–21] One category of molecular square or grid molecule makes use of nitrogen heterocyclic

* Author to whom correspondence should be addressed. E-mail: dunbar@mail.chem.tamu.edu.
[†] Texas A&M University.
[||] Present address: Department of Chemistry & Biochemistry, Florida State University, Tallahassee, FL 32306.
[‡] Florida State University.
[§] Roosevelt University.

(1) Steed, J. W.; Atwood, J. L. *Supramolecular Chemistry*; John Wiley & Sons: New York, 2000.
(2) Berlinguette, C. P.; Smith, J. A.; Galán-Mascarós, J. R.; Dunbar, K. R. *C. R. Chim.* **2002**, 665–672.
(3) Oshio, H.; Tamada, O.; Onodera, H.; Ito, T.; Ikoma, T.; Tero-Kubota, S. *Inorg. Chem.* **1999**, *38*, 5686–5689.
(4) Oshio, H.; Tamada, O.; Onodera, H.; Mizutani, H.; Hikichi, T.; Ito, T. *Chem.—Eur. J.* **2000**, *6*, 2523–2530.
(5) Kou, K.; Gao, S.; Li, C.; Liao, D.; Bei-Zhou, C.; Wang, R.; Li, Y. *Inorg. Chem.* **2002**, *41*, 4756–4762.
(6) Falvello, L. R.; Tomás, M. *Chem. Commun.* **1999**, 273–274.
(7) Klausmeyer, K. K.; Rauchfuss, T. B.; Wilson, S. R. *Angew. Chem., Int. Ed.* **1998**, *37*, 1694–1696.
(8) Darensbourg, D. J.; Lee, W.; Adams, M. J.; Yicbrough, J. C. *Eur. J. Inorg. Chem.* **2001**, 2811–2822.
(9) Oshio, H.; Yamamoto, M.; Ito, T. *Inorg. Chem.* **2002**, *41*, 5817–5820.
(10) Schinnerling, P.; Thewalt, U. *J. Organomet. Chem.* **1992**, *431*, 41–45.
(11) Flay, M.; Comte, V.; Vahrenkamp, H. *Z. Anorg. Allg. Chem.* **2003**, *629*, 1147–1152.
(12) Li, D.; Parkin, S.; Wang, G.; Yee, G. T.; Prosvirin, A. V.; Holmes, S. M. *Inorg. Chem.* **2005**, *44*, 4903–4905.
(13) Toma, L. M.; Lescouezec, R.; Cangussu, D.; Llusar, R.; Mata, J.; Spey, S.; Thomas, J. A.; Lloret, F.; Julve, M. *Inorg. Chem. Commun.* **2005**, *8*, 382–385.
(14) Yeung, W.-F.; Kwong, H.-K.; Lau, T.-C.; Gao, S.; Szeto, L.; Wong, W.-T. *Polyhedron* **2006**, *25*, 1256–1262.
(15) Kim, J.; Han, S.; Cho, I.-K.; Choi, K. Y.; Heu, M.; Yoon, S.; Suh, B. J. *Polyhedron* **2004**, *23*, 1333–1339.
(16) Li, D.; Parkin, S.; Wang, G.; Yee, G. T.; Holmes, S. M. *Inorg. Chem.* **2006**, *45*, 2773–2775.
(17) Li, D.; Parkin, S.; Wang, G.; Yee, G. T.; Holmes, S. M. *Inorg. Chem.* **2006**, *45*, 1951–1959.

10.1021/ic702084e CCC: $40.75
Published on Web 02/15/2008

ligands as the linker groups. For example, the bptz ligand (bptz = 3,6-bis(2-pyridyl)-1,2,4,5-tetrazine) gives rise to molecular squares and pentagons when octahedral metal ions are used as building blocks.[24–26]

Another important bridging group in the chemistry of molecular squares is the cyanide ion, which has been widely used as a linker to prepare magnetic molecules and materials since the cyanide linkage provides a short (~5.0 Å), efficient pathway for superexchange between metal ions.[27] Metal−cyanide squares composed of paramagnetic ions can yield molecules with high-spin ground states, which hold potential for the development of new molecules that exhibit interesting magnetic properties such as single-molecule magnetism.[2–21]

One reason for the interesting magnetic properties of molecular squares is the fact that all four metal ions of a molecular square reside approximately in the same plane, which reduces the cancelation of the local magnetic anisotropies of the metal ions and results in higher global anisotropy of the cluster.[22,23] In addition to the geometry of the entire cluster and of the linking group, another important parameter defining the magnetic behavior of the cluster is the coordination geometry at each metal center. Therefore, control and variation of the coordination environment around the metal centers represents an interesting avenue to explore. Provided that there are capping ligands present that exert a dominant influence on the geometry at the metal center, it is possible to realize a number of different clusters on the basis of a convergent building block approach.[2–21] The first reported tetranuclear cyanide-bridged cluster, to our knowledge, is the $[Cp_2Ti^{III}(CN)]_4$ square, which was prepared by Schinnerling and Thewalt, with cyclopentadienyl (Cp) capping ligands.[10] The cyclopentadienyl ligand was also used by other groups to yield Cp-capped molecular squares based on Rh_4[7] and Fe_2Cu_2[4] units. Complexes of bpy (2,2′-bipyridine) and phen (1,10-phenanthroline) have also been used by our group[28] and by Vahrenkamp et al.[11] and Oshio et al.[3,4,9]

The triphos ligand (triphos: 1,1,1-tris(diphenylphosphinomethyl)ethane) has been employed in our laboratory to prepare a family of cubic clusters based on the [(triphos)$Re(CN)_3]^-$ building block.[22,29,30] Given this success, we searched for convenient triphos-containing metal−cyanide compounds that could be used to prepare a series of magnetic molecular squares. A perusal of the literature revealed that there exists a five-coordinate paramagnetic complex (S = 1/2) with a square-pyramidal metal center, [Co^{II}(triphos)$(CN)_2$], synthesized by Rupp et al.,[31,32] with a C−Co−C bond angle of approximately 90°. Combination of this convergent precursor with divergent metal dichlorides led to a series of cyanide-linked molecular squares.[33] Herein, we report the synthesis and characterization of a homologous series of molecular squares based on the distorted square-pyramidal Co(II) complex and tetrahedral 3d metal ions.

Experimental Section

Syntheses. Starting Materials. Co(triphos)$(CN)_2$[31] and $Fe_4Cl_8(THF)_6$[34] were prepared according to the published procedures. The anhydrous starting materials $MnCl_2$, $CoCl_2$, $NiCl_2$, and $ZnCl_2$ were purchased from Aldrich and used as received.

{[Co(triphos)$(CN)_2]_2[MCl_2]_2$}·$x CH_2Cl_2$ (M = Mn, Co, Ni, and Zn; abbreviated throughout as [CoMn], [CoCo], [CoNi], and [CoZn], respectively; x = 3 or 4). In the case of **[CoMn]**, a claret solution of Co(triphos)$(CN)_2$ (100 mg, 0.136 mmol) in 30 mL of dichloromethane was slowly layered with a solution of $MnCl_2$ (34 mg, 0.270 mmol) in 30 mL of ethanol. The mixture was left to stand undisturbed for 3−4 days. Dark red crystals of **[CoMn]** that formed after 3 days were collected by filtration and washed with copious amounts of ethanol. Yield = 42 mg (40%). Elem anal. calcd for **[CoMn]**, $Co_2Mn_2C_{86}H_{78}N_4Cl_4$: C 63.37, H 3.36, N 3.44, Cl 8.70. Found: C 62.52, H 3.64, N 3.20, Cl 8.27%. IR (Nujol), ν(C≡N), cm^{-1}: 2119(s), 2101(w). Single crystals of **[CoMn]** were grown over a 1 week period in a closed, thin tube by slow diffusion of an EtOH solution of $MnCl_2$ into a CH_2Cl_2 solution of Co(triphos)$(CN)_2$. Compounds **[CoNi]** and **[CoZn]** were prepared in an analogous fashion to that described above for compound **[CoMn]**. Compound **[CoCo]** was washed with a CH_2Cl_2/EtOH (1:1) mixture several times, and the solution was decanted under N_2 without filtering. The yields were 65 mg (62%), 54 mg (52%), and 59 mg (56%), respectively. Elem anal. calcd for **[CoCo]**, $Co_4C_{86}H_{78}N_4Cl_4$: C 63.06, H 4.80, N 3.42, Cl 8.66. Found: C 62.81, H 4.53, N 3.24, Cl 8.20%. Elem anal. calcd for **[CoNi]**, $Co_2Ni_2C_{86}H_{78}N_4Cl_4$: C 63.10, H 4.80, N 3.42, Cl 8.66. Found: C 62.77, H 4.60, N 3.06, Cl 8.12%. Elem anal. calcd for **[CoZn]**, $Co_2Zn_2C_{86}H_{78}N_4Cl_4$: C 62.57, H 4.76, N 3.39, Cl 8.59. Found: C 62.28, H 4.68, N 3.19, Cl 8.31%. IR (Nujol), ν(C≡N), cm^{-1}: 2132(s), 2101(w) for **[CoCo]**; 2133(s), 2102(w) for **[CoNi]**; 2140(s), 2104(w) for **[CoZn]**. The single crystals of **[CoCo]**·$3CH_2Cl_2$, **[CoNi]**·$4CH_2Cl_2$, and **[CoZn]**·$4CH_2Cl_2$ were obtained in a similar manner to that described for compound **[CoMn]**.

{[Co(triphos)$(CN)_2]_2[FeCl_2]_2$}·$3CH_2Cl_2$ [CoFe]. A claret solution of Co(triphos)$(CN)_2$ (200 mg, 0.272 mmol) in 30 mL of dichloromethane was slowly layered with a solution of $Fe_4Cl_8(THF)_6$ (130 mg, 0.139 mmol) in 30 mL of ethanol under

(18) Liu, W.; Wang, C.; Li, Y.; Zuo, J.; You, X. *Inorg. Chem.* **2006**, *45*, 10058–10065.
(19) Rodriguez-Diéguez, A.; Kivekãs, R.; Sillanpãã, R.; Cano, J.; Lloret, F.; McKee, V.; Stoeckli-Evans, H.; Colacio, E. *Inorg. Chem.* **2006**, *45*, 10537–10551.
(20) Jiang, L.; Feng, X.; Lu, T.; Gao, S. *Inorg. Chem.* **2006**, *45*, 5018–5026.
(21) Rebilly, J.; Catala, L.; Charron, G.; Rogez, G.; Riviére, E.; Guillot, R.; Thuéry, P.; Barra, A.; Mallah, T. *Dalton Trans.* **2006**, 2818–2828.
(22) Schelter, E. J.; Karadas, F.; Avendano, C.; Prosvirin, A. V.; Wernsdorfer, W.; Dunbar, K. R. *J. Am. Chem. Soc.* **2007**, *129*, 8139–8149.
(23) Ruiz, D.; Sun, Z.; Albela, B.; Folting, K.; Ribas, J.; Christou, G.; Hendrickson, D. N. *Angew. Chem., Int. Ed.* **1998**, *37*, 300–302.
(24) Campos-Fernandez, C. S.; Clerac, R.; Dunbar, K. R. *Angew. Chem., Int. Ed.* **1999**, *38*, 3477–3479.
(25) Youinou, M.; Rahmouni, N.; Fischer, J.; Osborn, J. A. *Angew. Chem., Int. Ed.* **1992**, *31*, 733–735.
(26) Campos-Fernandez, C. S.; Clerac, R.; Koomen, J. M.; Russell, D. H.; Dunbar, K. R. *J. Am. Chem. Soc.* **2001**, *123*, 773–774.
(27) Dunbar, K. R.; Heintz, R. A. *Prog. Inorg. Chem.* **1997**, *45*, 283–391.
(28) Berlinguette, C. P.; Vaughn, D.; Cañada-Vilalta, C.; Galán-Mascarós, J.; Dunbar, K. R. *Angew. Chem., Int. Ed.* **2003**, *42*, 1523–1526.
(29) Schelter, E. J.; Prosvirin, A. V.; Dunbar, K. R. *J. Am. Chem. Soc.* **2004**, *126*, 15004–15005.
(30) Schelter, E. J.; Prosvirin, A. V.; Reiff, W. M.; Dunbar, K. R. *Angew. Chem., Int. Ed.* **2004**, *43*, 4912–4915.
(31) Rupp, R.; Huttner, G.; Kircher, P.; Soltek, R.; Buchner, M. *Eur. J. Inorg. Chem.* **2000**, 1745–1757.
(32) Jacob, V.; Mann, S.; Huttner, G.; Walter, O.; Zsolnai, L.; Kaifer, E.; Rutsch, P.; Kircher, P.; Bill, E. *Eur. J. Inorg. Chem.* **2001**, 2625–2640.
(33) Karadas, F.; Schelter, E. J.; Prosvirin, A. V.; Bacsa, J.; Dunbar, K. R. *Chem. Comm.* **2005**, 1414–1416.
(34) Cotton, F. A.; Luck, R. L.; Son, K. A. *Inorg. Chim. Acta* **1991**, *179*, 11–15.

Table 1. Crystal Data and Details of the Structure Determination for **[CoM]** Square Compounds

Formula	$Co_2Mn_2C_{86}H_{78}N_4Cl_4$ (**[CoMn]**·$3CH_2Cl_2$)	$Co_2Fe_2C_{86}H_{78}N_4Cl_4$ (**[CoFe]**·$3CH_2Cl_2$)	$Co_4C_{86}H_{78}N_4Cl_4$ (**[CoCo]**·$3CH_2Cl_2$)	$Co_2Ni_2C_{86}H_{78}N_4Cl_4$ (**[CoNi]**·$4CH_2Cl_2$)	$Co_2Zn_2C_{86}H_{78}N_4Cl_4$ (**[CoZn]**·$4CH_2Cl_2$)
space group	$P2_1/n$ (No. 14)	$P2_1/n$ (No. 14)	$P2_1/n$ (No. 14)	$P2_1/n$ (No. 14)	$P2_1/n$ (No. 14)
unit cell	a = 14.079(3) Å	a = 13.998(3) Å	a = 14.193(5) Å	a = 14.085(3) Å	a = 13.930(2) Å
monoclinic	b = 16.444(4) Å	b = 16.412(4) Å	b = 16.481(6) Å	b = 16.365(3) Å	b = 49.141(8) Å
	c = 19.995(5) Å	c = 19.929(5) Å	c = 19.750(7) Å	c = 19.875(4) Å	c = 19.890(3) Å
	β = 90.129(4)°	β = 90.166(7)°	β = 90.366(7)°	β = 90.10(3)°	β = 90.004(3)°
unit cell volume, V	4629(8) Å^3	4578.2(19) Å^3	4620(3) Å^3	4581.5(16) Å^3	13616(4) Å^3
Z	2	2	2	2	6
density, ρ_{calc}	1.480 g/cm^3	1.436 g/cm^3	1.489 g/cm^3	1.254 g/cm^3	1.276 g/cm^3
abs. coeff., μ	1.116 mm^{-1}	1.109 mm^{-1}	1.204 mm^{-1}	1.024 mm^{-1}	1.147 mm^{-1}
cryst color and habit	dark-red plate	blue plate	green-blue plate	blue plate	brown plate
cryst size	0.30 × 0.30 × 0.03 mm	0.39 × 0.27 × 0.21 mm	0.32 × 0.22 × 0.19 mm	0.34 × 0.32 × 0.26 mm	0.27 × 0.18 × 0.11 mm
temperature	110(2) K	110(2) K	100(2) K	110(2) K	100(2) K
radiation, λ	Mo Kα, 0.71073 Å	Mo Kα, 0.71073 Å	Mo Kα, 0.71073 Å	Mo Kα, 0.71073 Å	Mo Kα, 0.71073 Å
min. and max. θ	2.48−27.48°	1.02−27.48°	2.06−28.41°	2.17−27.62°	1.10−28.35°
reflns collected	45463 [R_{int} = 0.1465]	21456 [R_{int} = 0.0688]	38562 [R_{int} = 0.0656]	27965 [R_{int} = 0.0654]	139897 [R_{int} = 0.1004]
independent reflns	10446	9596	10853	10853	10853
data/parameters/restraints	10446/502/12	9596/565/70	10853/563/8	9799/496/12	33158/1408/0
R [$F_o > 4\sigma(F_o)$]	R_1 = 0.0697	R_1 = 0.0721	R_1 = 0.0653	R_1 = 0.0554	R_1 = 0.1015
	wR_2 = 0.1566	wR_2 = 0.1778	wR_2 = 0.1502	wR_2 = 0.1368	wR_2 = 0.2592

N_2. The mixture was left to stand undisturbed for 2–3 days. Blue-red crystals of **[CoFe]** that formed over the course of 3 days were collected by filtration and washed with copious amounts of ethanol. Yield = 38 mg (36%). Elem anal. calcd for **[CoFe]**, $Co_2Fe_2C_{86}H_{78}N_4Cl_4$: C 63.30, H 4.82, N 3.43, Cl 8.69. Found: C 62.82, H 4.62, N 3.28, Cl 8.33%. IR (Nujol), ν(C≡N), cm^{-1}: 2120(s), 2101(w). Single crystals of compound **[CoFe]** were grown over a 1 week period in a closed thin tube by slow diffusion of an EtOH solution of $Fe_4Cl_8(THF)_6$ into a CH_2Cl_2 solution of Co(triphos)-$(CN)_2$.

Physical Measurements. Elemental analyses were performed by Atlantic Microlab, Inc. IR spectra were measured as Nujol mulls placed between KBr plates on a Nicolet 740 FT-IR spectrometer. Magnetic measurements were performed on freshly prepared crushed polycrystalline samples with a Quantum Design SQUID MPMS-XL magnetometer. DC magnetic susceptibility measurements were carried out in an applied field of 1000 Oe in the 2–300 K range. Magnetization data were collected at 1.8 K with the magnetic field varying from 0 to 70 kOe. The reduced magnetization data were collected in the 1.8–3.9 K temperature range with the field varying from 10 to 70 kOe. AC magnetic susceptibility measurements were performed with a 3 Oe AC driving field in an operating frequency range of 1–1000 Hz. The data were corrected for the diamagnetic contributions calculated from Pascal's constants.

X-Ray Crystallography. In a typical experiment, a crystal selected for study was suspended in polybutene oil (Aldrich) and mounted on a cryoloop which was placed in a N_2 cold stream. Single-crystal X-ray data for all the compounds were collected on a Bruker APEX diffractometer at 110 K. The data sets were recorded as three ω scans of 606 frames each, at a 0.3° stepwidth, and integrated with the Bruker SAINT[35] software package. For each compound, the data set was indexed in a monoclinic unit cell and systematic extinctions indicated the space group to be $P2_1/n$. The absorption correction (SADABS[36]) was based on fitting a function to the empirical transmission surface as sampled by multiple equivalent measurements. Solution and refinement of the crystal structures was carried out using the SHELX[37] suite of programs and X-SEED,[38] a graphical interface. Structure solution by direct methods resolved positions of all metal atoms and most of the lighter atoms. The remaining nonhydrogen atoms were located by alternating cycles of least-squares refinements and difference Fourier maps. The option SQUEEZE in PLATON[39] was used to eliminate the contribution of the electron density in the solvent region from the intensity data. The use of SQUEEZE produced better refinement results, and the solvent-free model was employed for the final refinement. Hydrogen atoms were placed at calculated positions and refined with displacement parameters 1.2 or 1.5 times that of the heavy atoms to which they were bonded. The final refinement was performed with anisotropic thermal parameters for all nonhydrogen atoms. A summary of pertinent information relating to unit cell parameters, data collection, and refinements are provided in Table 1. Selected metal–ligand bond distances are provided in Table 2. Complete listings of atomic and thermal parameters, bond distances, and bond angles are available as Supporting Information.

High-Frequency and -Field Electron Paramagnetic Resonance (HFEPR). All of the **[CoM]** molecular square complexes were investigated by HFEPR using either the Millimeter and Sub-mm Wave Facility[40] or the EMR Facility[41] at the National High Magnetic Field Laboratory. The former experimental setup employs tunable frequencies in the 150–700 GHz range generated by backward wave oscillators and the resistive "Keck" magnet enabling 0–25 T field sweeps. The latter spectrometer is based on a 17 T superconducting magnet and uses a 13 ± 1 GHz base frequency source (Virginia Diodes Inc., Charlottesville, VA) followed by an amplifier and a series of frequency multipliers, thus providing EPR spectra at intermediate frequencies, for example, V-band (48 – 56 GHz), as well as at high frequencies. Detection was effected with an InSb hot-electron bolometer (QMC Ltd., Cardiff, U.K.). Modulation for detection purposes was provided alternatively by chopping the sub-THz wave beam ("optical modulation") or by modulating the magnetic field. A Stanford Research Systems SR830 lock-in amplifier converted the modulated signal to DC voltage. Typically, 30–50 mg of polycrystalline sample was used in either experiment.

(35) *SMART and SAINT*; Siemens Analytical X-ray Instruments Inc.: Madison, WI, **1996**.
(36) Sheldrick, G. M. *SADABS*; University of Göttingen: Göttingen, Germany, **1996**.
(37) Sheldrick, G. M. *SHELXS-97*; *SHELXL-97*; University of Göttingen: Göttingen, Germany, **1997**.
(38) Barbour, L. J. *J. Supramol. Chem.* **2001**, *1*, 189–191.
(39) Van der Sluis, P.; Spek, A. L. *Acta Crystallogr., Sect. A* **1990**, *46*, 194–201.
(40) Zvyagin, S. A.; Krzystek, J.; van Loosdrecht, P. H. M.; Dhalenne, G.; Revcolevschi, A. *Physica B (Amsterdam, Neth.)* **2004**, *346–347*, 1–5.
(41) Hassan, A. K.; Pardi, L. A.; Krzystek, J.; Sienkiewicz, A.; Goy, P.; Rohrer, M.; Brunel, L. C *J. Magn. Reson.* **2000**, *142*, 300–312.

Table 2. Selected Bond Distances (Å) and Angles for **[CoM]** Square Compounds

parameters	[CoMn]	[CoFe]	[CoCo]	[CoNi]	[CoZn]
Co1−C1	1.875(5)	1.894(5)	1.887(4)	1.883(4)	1.890(7)
Co1−C2	1.894(5)	1.894(5)	1.886(4)	1.885(4)	1.882(7)
Co1−P1	2.215(2)	2.2281(15)	2.2173(13)	2.3156(13)	2.2364(18)
Co1−P2	2.2875(19)	2.2436(16)	2.2955(12)	2.2424(11)	2.2978(19)
Co1−P3	2.239(2)	2.2855(17)	2.2368(12)	2.2115(11)	2.2324(18)
M1−N1	2.083(5)	2.028(4)	1.983(3)	1.981(3)	2.009(5)
M1−N2	2.077(4)	2.029(4)	1.989(4)	1.992(3)	1.995(6)
M1−Cl1	2.308(2)	2.2597(18)	2.2346(14)	2.2343(13)	2.2525(19)
M1−Cl2	2.336(2)	2.2691(18)	2.2569(13)	2.2407(14)	2.230(2)
C1−Co1−C2	84.87(17)	85.18(19)	84.98(15)	84.47(14)	84.8(3)
C1−Co1−P1	160.52(15)	161.24(17)	160.89(12)	157.88(12)	161.9(2)
C2−Co1−P1	89.41(14)	89.48(14)	89.56(12)	89.44(11)	89.0(2)
C1−Co1−P3	91.65(13)	91.46(15)	91.81(11)	91.47(10)	91.65(19)
C2−Co1−P3	167.75(15)	168.00(17)	167.94(12)	166.96(13)	167.4(2)
P1−Co1−P3	90.02(5)	90.07(6)	89.74(4)	89.72(4)	90.93(7)
C1−Co1−P2	107.77(16)	107.73(17)	107.82(12)	110.26(12)	106.36(19)
C2−Co1−P2	101.76(16)	101.97(16)	102.11(12)	102.91(12)	102.2(2)
P1−Co1−P2	91.62(8)	90.96(6)	91.23(5)	91.83(4)	91.65(19)
P3−Co1−P2	90.48(7)	90.03(6)	89.95(4)	90.12(4)	90.67(7)
N2−M1−N1	103.16(14)	101.49(16)	105.15(13)	104.39(12)	102.3(2)
N2−M1−Cl1	116.22(12)	115.07(13)	115.51(10)	115.24(10)	114.99(17)
N1−M1−Cl1	104.72(12)	104.56(14)	106.21(10)	105.41(10)	106.35(18)
N2−M1−Cl2	107.52(14)	107.02(13)	107.13(10)	107.36(10)	108.27(17)
N1−M1−Cl2	106.49(13)	107.13(14)	106.39(10)	107.28(10)	107.27(17)
Cl1−M1−Cl2	117.29(6)	119.70(6)	115.58(5)	116.24(5)	116.44(8)
C1−N1−M1	172.6(4)	173.5(5)	175.3(3)	175.2(3)	173.3(5)
N1−C1−Co1	176.0(4)	173.8(5)	173.0(3)	174.6(3)	174.8(6)
C2−N2−M1	173.2(4)	173.9(4)	173.0(3)	173.8(3)	173.0(5)
N2−C2−Co1	175.4(4)	175.8(4)	175.2(4)	175.7(3)	176.2(6)

Additional X-band measurements were performed on **[CoZn]** using a commercial Bruker E680X spectrometer.

Results and Discussion

Syntheses. The Co(II) center exhibits a square-pyramidal geometry, which is typical for most phosphine complexes of Co(II), including those with chelating and monodentate phosphine ligands.[42] The presence of a capping triphos ligand and two cyanide ligands positioned at a C−Co−C angle of 87.6° renders this compound a convenient precursor for the assembly of molecular squares. The C−Co−C angle is smaller than C−Co−C angles in a homoleptic square-pyramidal anion $[Co(CN)_5]^{3-}$ (88.6–99.6°).[43] This decrease is attributed to the steric effect of the bulky triphos ligand in the Co(triphos)$(CN)_2$ complex.

A claret solution of Co(triphos)$(CN)_2$ in dichloromethane was reacted with solutions of MCl_2 (M = Mn, Co, Ni, and Zn) or $Fe_4Cl_8(THF)_6$ in ethanol to form the title compounds. In the case of **[CoFe]**, $Fe_4Cl_8(THF)_6$ was used instead of $FeCl_2$, since the THF solvate is a purer form of ferrous chloride and thus is an excellent source of Fe(II) for substitution chemistry. The compounds are stable both in solution and in the solid phase, except for **[CoFe]**, which is air-sensitive. Also, **[CoCo]** shows a degree of decomposition during the drying process, which is described in the magnetism section. The complexes are nearly insoluble in common solvents such as CH_2Cl_2, MeOH, hexane, and MeCN. They are soluble only in DMF and slightly soluble in propylene carbonate.

Single Crystal X-Ray Structures. Single crystals of the products were prepared by slow diffusion of an EtOH solution of MCl_2 into a CH_2Cl_2 solution of Co(triphos)$(CN)_2$. The molecular squares are composed of alternating Co(triphos)$(CN)_2$ and MCl_2 units (Figure 1). The molecule crystallizes on an inversion center, so that the asymmetric unit is composed of one-half of the square. The Co(II) sites remain pentacoordinate, with only slight changes to the metal–ligand coordination sphere as compared to the starting material. The C−Co−C angle is similar in all of the structures (∼85°, Table 2). The coordination geometry around the M(II) sites is distorted tetrahedral and consists of two N atoms of the cyanide groups and two Cl^- ions. The distorted tetrahedral environment of the M(II) sites is primarily related to the steric demand of the triphos ligand. The N−M−N angles vary between 101.5(2)° and 105.2(1)°.

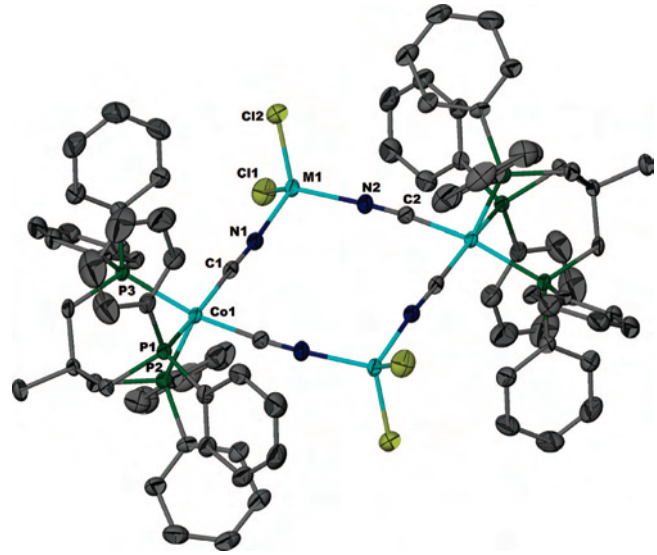

Figure 1. Structure of **[CoM]** squares where M = Mn, Fe, Co, Ni, Zn.

(42) Rigo, P.; Turco, A. *Coord. Chem. Rev.* **1974**, *13*, 133–172.
(43) Brown, L. D.; Raymond, K. N. *Inorg. Chem.* **1975**, *14*, 2590–2594.

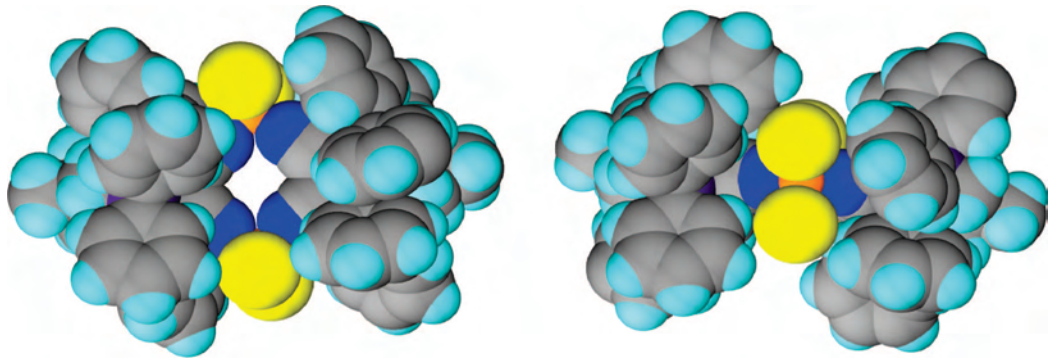

Figure 2. Space-filling diagrams of the squares depicted from the top and the side.

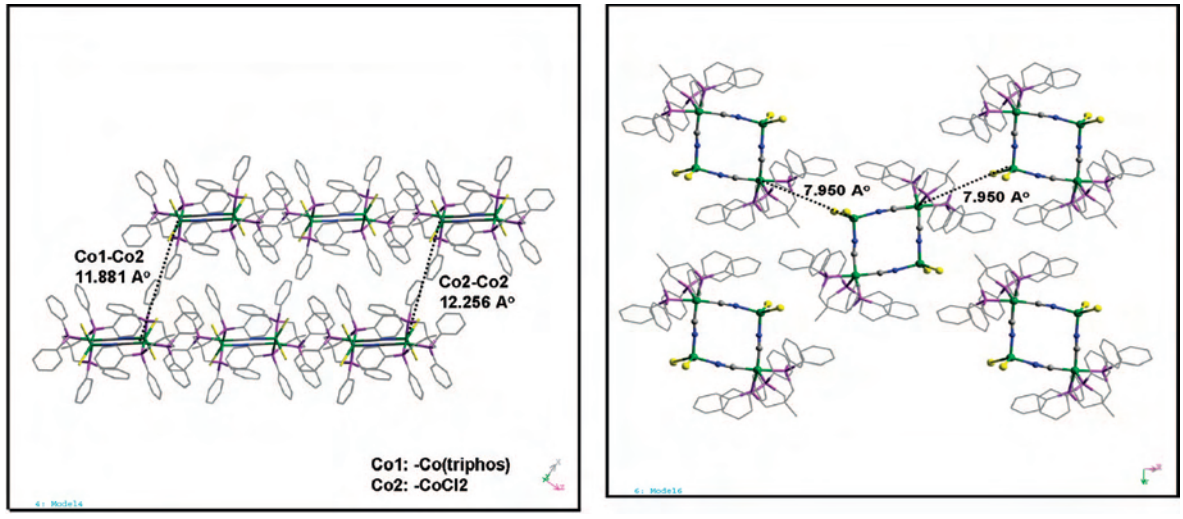

Figure 3. Packing diagrams for compound **[CoCo]**. The intermolecular Co···Co distances are labeled in both figures. The left figure lists the Co···Co distances between the layers, while the right figure indicates the distances within the layer.

The combination of square-pyramidal and tetrahedral metal centers results in a more distorted molecular square as compared to those based on octahedrally coordinated metal ions. For example, the previously reported $Fe^{III}Ni^{II}$ square, $[Tp^*Fe^{III}(CN)_3Ni^{II}(DMF)_4]_2[OTf]_2$,[12] exhibits C−$Fe^{III}$−C and N−$Ni^{II}$−N angles of 86.8(2)° and 92.3(1)°, respectively, and the $Fe^{II}Co^{II}$ square, $[Fe^{II}Co^{II}(\mu\text{-CN})(bpy)_8](PF_6)_4$,[4] has C−$Fe^{II}$−C and N−$Co^{II}$−N angles equal to 91.9(1)° and 91.2(2)°, respectively. Also, space-filling diagrams of the squares clearly indicate that the chloride atoms attached to M(II) are still readily accessible for further substitution reactions with cyanide precursors, although the bulk of the triphos ligand distorts the structure (Figure 2).

In all of the **[CoM]** complexes, the crystal structures indicate that there are no obvious pathways for intermolecular magnetic communication among metal centers, as there is neither H bonding nor any apparent strong dipolar interaction since the shortest intermolecular M···M distance in, for example, **[CoCo]** is 7.950 Å (Figure 3).

Infrared Spectroscopy. Infrared spectroscopy performed on polycrystalline samples of the products reveals two $\nu_{C\equiv N}$ stretches, located at 2119(s) and 2101 cm^{-1} in compound **[CoMn]**, 2120(s) and 2101(w) cm^{-1} in **[CoFe]**, 2132(s) and 2101(w) cm^{-1} in **[CoCo]**, 2133(s) and 2100(w) cm^{-1} in **[CoNi]**, and 2140(s) and 2104(w) cm^{-1} in **[CoZn]**. There is a positive shift of 23, 24, 36, 37, and 44 cm^{-1}, respectively, as compared to the starting material, for which the $\nu_{C\equiv N}$ stretches are located at 2096(s) and 2101(w) cm^{-1}. A shift to higher frequencies is a clear indication of the formation of a bridging cyanide mode.[32] Most of the reported molecular squares exhibit similar C≡N modes, with either one or two bands depending on the symmetry of the molecule. For example, the $Fe^{II}Cu^{I}$ square, $[CpFe(CO)(\mu\text{-CN})_2Cu(PMePh_2)_2]_2$,[8] exhibits two $\nu_{C\equiv N}$ stretches, located at 2110 and 2095 cm^{-1}.

Magnetic Studies. DC magnetic susceptibility measurements for the molecular square compounds and the mononuclear building block, $Co(triphos)(CN)_2$, were performed on freshly prepared crushed polycrystalline samples in the temperature range of 2–300 K at an applied magnetic field of 1 kOe. The χT versus T plots are depicted in Figure 4. For the mononuclear starting material, $Co(triphos)(CN)_2$, the value of χT at 300 K is 0.41 emu·mol^{-1}·K and remains constant over the entire temperature range, typical of a simple paramagnet with an $S = 1/2$ spin ground-state and $g = 2.10$. This is comparable to the magnetic properties of other square-pyramidal Co(II) phosphine complexes such as $Co(PPh_2Et)_3(CN)_2$, $Co(PPh_2Me)_3(CN)_2$, $Co(dpe)_2(CN)_2$, and $Co(HPPh_2)_3(CN)_2$.[42]

For the square compounds, we first consider **[CoZn]**, in which the presence of diamagnetic Zn(II) results in a simple paramagnet composed of two mononuclear $Co(triphos)(CN)_2$

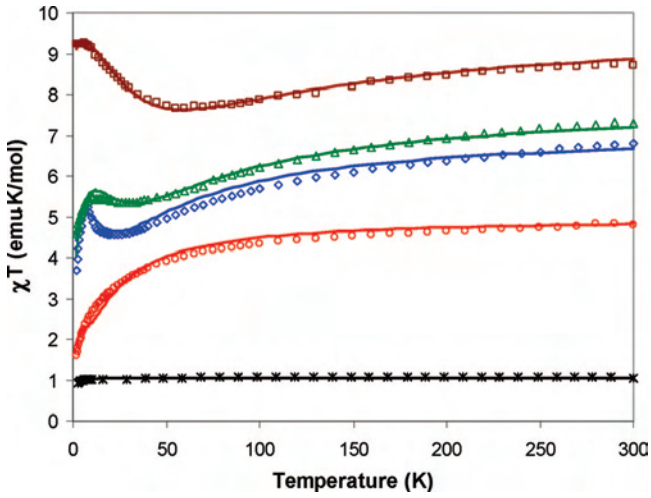

Figure 4. Temperature dependence of the χT product for compounds **[CoMn]** (□), **[CoFe]** (Δ), **[CoCo]** (◊), **[CoNi]** (○), and **[CoZn]** (*). The solid lines correspond to the simulation with the use of the MAGPACK program according to eq 2 (see text).

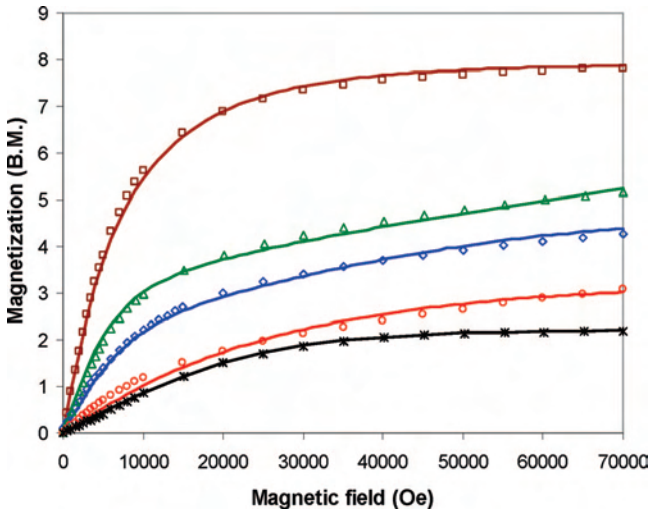

Figure 5. Field-dependent magnetization curves for compounds **[CoMn]** (□), **[CoFe]** (Δ), **[CoCo]** (◊), **[CoNi]** (○), and **[CoZn]** (*) measured at 1.8 K. The solid lines correspond to the simulation with the use of the MAGPACK program according to eq 1 (see text).

units per cluster. The value of χT at 300 K is 1.05 emu·mol^{-1}·K and remains constant over the whole temperature interval for this cluster. A plot of χT versus T obeys the Curie law (Figure 4). Field-dependent magnetization data are fit to a Brillouin function for two isolated centers with $S = 1/2$ (Figure 5). The calculated values are listed in Table 3. The data indicate an absence of magnetic interaction between the two low-spin Co(II) ions in the molecular square, which allows us to make the assumption that the magnetic interaction between the two Co(II) centers in the diagonally opposite corners of the square can be neglected. This assumption will be used when treating magnetic data for the other square compounds in this work. Magnetic measurements on the other compounds, in which all four metal ions are paramagnetic, gave evidence of strong magnetic interactions between adjacent ions.

In the case of the **[CoMn]** compound, the DC susceptibility studies revealed a value of $\chi T = 8.7$ emu·mol^{-1}·K at 300 K, which is considerably lower than the spin-only value of 9.5 emu·mol^{-1}·K expected for two Co(triphos)$(CN)_2$ units ($S = 1/2$, $\chi T = 0.41$) and two Mn(II) ions ($S = 5/2$) in the absence of magnetic coupling. The value of χT decreases upon cooling until $T \sim 65$ K, below which χT abruptly increases to reach a maximum of 9.96 emu·mol^{-1}·K at 6 K. The decrease of χT between 300 and 65 K indicates the presence of antiferromagnetic (AF) interactions between the two $S = 1/2$ Co(II) and the two $S = 5/2$ Mn(II) ions. The observed maximum for the $\chi_m T$ product at 6 K is indicative of the stabilization of an $S = 4$ ground state, whereas the decrease at lower temperatures (2–6 K) is attributed to zero-field splitting (zfs) effects. An examination of the ground spin state for **[CoMn]** was carried out by performing the magnetization measurements at different temperatures in order to determine the zfs parameters more accurately. The data were fit using the program ANISOFIT,[44] where the best fit was obtained by applying the following Hamiltonian with the parameters $S_{total} = 4$, $g = 1.95$, and $D = -0.24$ cm^{-1} (where D is the axial zfs parameter; Figure S1, Supporting Information).

$$\mathscr{H} = \mu_B H \cdot \mathbf{g} \cdot \hat{S} + D[\hat{S}_z^2 - (1/3)S(S+1)] \quad (1)$$

Field-dependent magnetization measured at 1.8 K in the field range of 0–70 kOe approaches a value of 7.86 μ_B, which is also in good agreement with the expected ground-state spin value from AF coupling; $S_{total} = S_{Mn1} - S_{Co1} + S_{Mn2} - S_{Co2} = 4$ (8 μ_B) (Figure 5). An acceptable model for the magnetization of **[CoMn]** was achieved using MAGPACK,[45,46] by applying the above Hamiltonian for the low-temperature behavior using the same values for the magnetic parameters obtained from the DC susceptibility measurement. Simulations of the χT versus T data using MAGPACK also allowed for estimations of g(Mn) and exchange parameter J. A spin-Hamiltonian was constructed in the limit of an isotropic exchange interaction, and contains only one J value, taking advantage of the molecular symmetry (eq 2).

$$\mathscr{H} = 2\mu_B H \cdot (\mathbf{g}_{CoCo} \cdot \hat{S}_{Co} + \mathbf{g}_{MM} \cdot \hat{S}_M) - 2J(\hat{S}_{Co1} + \hat{S}_{Co2})(\hat{S}_{M1} + \hat{S}_{M2}) + D_{M1}[\hat{S}_{z,M1} - (1/3)S_{M1}(S_{M1}+1)] + D_{M2}[\hat{S}_{z,M2}{}^2 - (1/3)S_{M2}(S_{M2}+1)] \quad (2)$$

All the terms given in eq 2 have their usual meanings; $\hat{S}$ refers to the spin operator of the appropriate metal ion, where index Co refers to (Co^{II}triphos) and indexes M1 and M2 refer to the tetrahedral Mn(II) ions, in this case Mn(II). The zero-field-splitting parameters of M1 and M2 were set equal to each other based on the molecular symmetry. The calculated values are listed in Table 3. Each low-spin Co(II) center is assigned the parameters $S = 1/2$ and $g = 2.10$ on the basis of magnetometry measurements.

For the **[CoFe]** compound, the value of χT at 300 K is 7.3 emu·mol^{-1}·K and decreases upon cooling, which indicates the presence of an antiferromagnetic interaction

(44) Shores, M. P.; Sokol, J. J.; Long, J. R. *J. Am. Chem. Soc.* **2002**, *124*, 2279–2292.
(45) Borras-Almenar, J. J.; Clemente-Juan, J. M.; Coronado, E.; Tsukerblat, B. S. *J. Comput. Chem.* **2001**, *22*, 985–991.
(46) Borras-Almenar, J. J.; Clemente-Juan, J. M.; Kou, H.-Z.; Gao, S.; Jin, X. *Inorg. Chem.* **2001**, *40*, 6295.

Table 3. Magnetic Properties of **[CoM]** Square Compounds

Compd	M(II)	$S_{M(II)}$	$g_{M(II)}$	J (cm^{-1})[a]	spin ground state, S_{total}	D (cm^{-1}) (magnetometry)[b]	D (cm^{-1}) (HFEPR)	E (cm^{-1}) (HFEPR)
[CoMn]	Mn	5/2	2.02	−10	4	−0.24	−0.22[c]	−0.009[c]
[CoFe]	Fe	2	2.12	−9	3	−2.98	*d*	*d*
[CoCo]	Co	3/2	2.40[e]	−8.0	2	−2.74	*d*	*d*
[CoNi]	Ni	1	2.8[f]	−6	1	−6	*d*	*d*
[CoZn][g]	Zn	0	0	∼0	2 × (S = 1/2)	0	0	0

[a] The $-2J$ formalism is employed. [b] Determined by fitting of DC susceptibility and field-dependent magnetization data, except for **[CoNi]**, where only magnetization fits were successful. [c] Determined by fits of single-frequency HFEPR spectra. [d] HFEPR results for **[CoCo]**, **[CoNi]**, and **[CoFe]** complexes were inconclusive. Studies of **[CoFe]** were further complicated by its being very air-sensitive. [e] This g value is reasonable for tetrahedral Co(II). For example, g = 2.248 for Co(II) in ZnS(β) (see ref 47, p 470); g = 2.23 for $[Co(NCS)_4]^{2-}$, and g = 2.48 for $[CoBr_4]^{2-}$ (see ref 52, p 218). [f] This g value is unusually high and is likely related to the fact that fits for this compound were problematic, as described in the text. [g] The compound **[CoZn]** exhibited magnetic behavior of two isolated S = 1/2 systems. Low- and intermediate-frequency EPR (9.4 and 52.8 GHz, respectively) was used in this case.

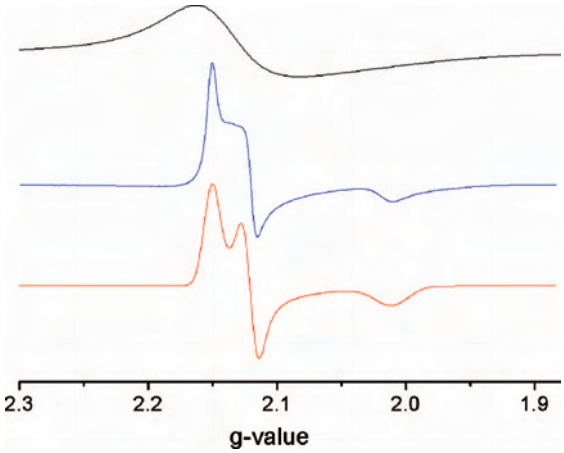

Figure 6. X-band (9.40 GHz, black trace) and V-band (52.8 GHz, blue trace) EPR spectra of **[CoZn]** at 4.2 K normalized with respect to the g value. The red trace is a powder simulation of the V-band spectrum using the following spin Hamiltonian parameters: S = 1/2, g_x = 2.15, g_y = 2.12, g_z = 2.01.

between the Co(II) and Fe(II) (S = 2) ions. Below 30 K, the value increases to reach a maximum of 5.5 emu·mol^{-1}·K at 9 K and then decreases at lower temperatures. An examination of the ground state for **[CoFe]** by ANISOFIT yielded the parameters S_{total} = 3, g = 2.04, and D = −2.98 cm^{-1} (Figure S2, Supporting Information). Field-dependent magnetization data and simulation using eq 1 are shown in Figure 5. Plots of the χT versus T and simulation using eq 2 are depicted in Figure 4. The calculated values are listed in Table 3. The total cluster spin value, S_{total} = 3 for **[CoFe]**, arises in the same way as that found for **[CoMn]**. The spins of the Co(II) ions are antiferromagnetically coupled to those of the M(II) ions: $S_{total} = S_{Fe1} - S_{Co1} + S_{Fe2} - S_{Co2}$.

For the **[CoCo]** compound, the value of χT at 300 K is 6.8 emu·mol^{-1}·K and decreases upon cooling, an indication of antiferromagnetic coupling between the low-spin (S = 1/2) and high-spin (S = 3/2) Co(II) ions. Below 20 K, the χT value increases to reach a maximum of 5.2 emu·mol^{-1}·K, which indicates the stabilization of the S_{total} = 2 ground state, and finally decreases below 7 K. An examination of the ground state by ANISOFIT yielded the parameters S_{total} = 2, g = 2.37, and D = − 2.74 cm^{-1} (Figure S3, Supporting Information). Field-dependent magnetization data and simulation using eq 1 are shown in Figure 6. Plots of χT versus T and simulation using eq 2 are shown in Figure 4. The calculated values are listed in Table 3.

The **[CoCo]** complex, as measured by AC susceptibility in its mother liquor, shows no indication of relaxation phenomena, as expected for isolated paramagnets. The **[CoCo]** complex that has been thoroughly dried in the air, however, exhibits a weak, frequency-dependent out-of-phase signal. The dried compound also exhibits a narrow hysteresis loop at 1.8 K, with a coercivity of ∼300 Oe and remnant magnetization of 0.1 μ_B, These results indicate that decomposition of some, or all, of the sample occurs during the drying process. The decomposition product of **[CoCo]** is unknown but must involve intermolecular interactions.

For the **[CoNi]** compound, the value of χT at 300 K is 4.8 emu·mol^{-1}·K and continuously decreases upon cooling, which indicates the presence of an antiferromagnetic interaction between the Co(II) and Ni(II) ions. Analysis of the ground state for **[CoNi]** by ANISOFIT failed to give satisfactory results (Figure S4, Supporting Information). The best fit to 1.8 K field-dependent magnetization data was obtained with MAGPACK using parameters S = 1, g = 2.57, and D = −6 cm^{-1} (Figure 5), although the quality of the fit is not very good. The reason for the poor fit could be the presence of low-lying excited states, which arise due to single-ion zfs and spin–orbit coupling effects. Plots of the χT versus T and the simulation using eq 2 are shown in Figure 4. The calculated values are listed in Table 3. A g value of approximately 2.8 for the Ni(II) ion is obtained when the data are fit assuming antiferromagnetic coupling between the Co(II) and Ni(II) centers. This g value is rather high for a tetrahedral Ni(II) ion ($g \approx 2.2$ is typical),[47] which also can be explained by the presence of low-lying excited states, leading to the higher effective g value. That the J and D parameters are of the same magnitude could contribute to the difficulty encountered in fitting the data.

EPR Studies. Low-temperature EPR spectra of **[CoZn]** are depicted in Figure 6, recorded at conventional, X-band (9.4 GHz), and intermediate-frequency, V-band (52.8 GHz), conditions. While the X-band spectrum consists of a single unresolved line, V-band EPR offers a vastly increased spectral resolution. The V-band spectrum can be adequately simulated assuming a powder distribution of crystallites and using S = 1/2, g_x = 2.15, g_y = 2.12, and g_z = 2.01. The average g value is 2.10, which agrees well with magnetic measurements that gave an isotropic g = 2.10. These g matrix values are characteristic for mononuclear low-spin Co(II) complexes, confirming the lack of significant magnetic exchange between the Co(II) moieties in the complex (The

(47) Abragam, A.; Bleaney, B. *Electron Paramagnetic Resonance of Transition Ions*; Dover Publications, Inc.: New York, 1986.

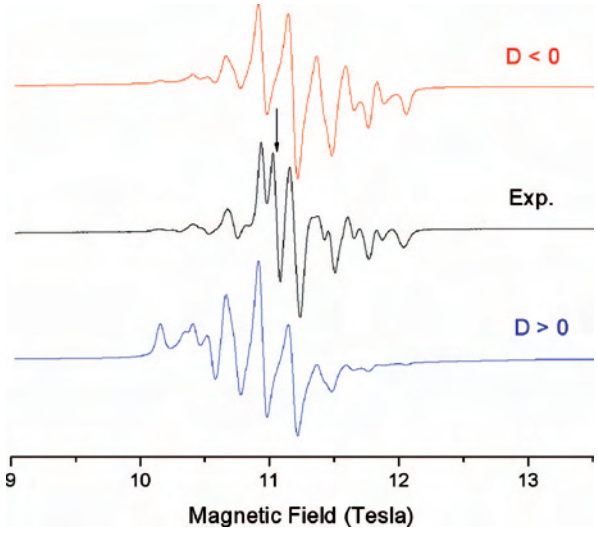

Figure 7. Representative HFEPR spectrum of **[CoMn]** at 309.6 GHz and 40 K. Black trace: experiment. Red trace: simulation using parameters $S = 4$, $D = -0.22$ cm^{-1}, $E = -0.009$ cm^{-1}, $g_{\perp} = 1.995$, $g_{\parallel} = 2.000$. Blue trace: simulation using positive zfs parameters of the same magnitude. The experimental spectrum contains an extra resonance at $g = 2.00$ possibly originating from free (i.e., uncoupled to other metal ions) Mn(II), indicated by the arrow, which is not reproduced in the simulation.

X- and V-band EPR spectra of the mononuclear complex Co(triphos)$(CN)_2$ were measured as well, and the spectra are shown in Figure S5, Supporting Information). Given that the g values of low-spin Co(II) are very sensitive to the coordination environment[42] and the geometry of the tripodal Co(triphos) complex is not identical to that in the **[CoZn]** square, there can easily be a shift in the g values, in this case producing less rhombicity in **[CoZn]** than in the starting complex.

The other molecular square complexes, containing exclusively paramagnetic single ions and exhibiting net integer spin ground states, were investigated by HFEPR at low temperatures (generally 5 K, and in some cases up to 40 K). Of these, only the **[CoMn]** complex gave informative results. A possible reason for this will be given below.

An exemplary spectrum for **[CoMn]** recorded at 310 GHz and 40 K is shown in Figure 7 together with its simulation assuming a powder distribution of crystallites in the sample. The spectrum was analyzed and simulated using the standard spin Hamiltonian given in eq 3, which is the same as in eq 1 but includes the transverse anisotropy parameter E of the cluster:[48]

$$\mathscr{H} = \mu_B H \cdot \mathbf{g} \cdot \hat{S} + D[\hat{S}_z - (1/3)S(S+1)] + E[\hat{S}_x^2 - \hat{S}_y^2] \quad (3)$$

The simulation unequivocally confirmed the $S_{total} = 4$ ground state of the complex and determined its spin Hamiltonian parameters. The obtained value of the zfs parameter $D = -0.22$ cm^{-1} (the negative sign being established through simulations, see Figure 7) is within 10% of the D value obtained from magnetometry. Magnetometry is generally insensitive to E, in contrast to HFEPR, a magnetic resonance technique.[49] Thus, a small rhombicity of the zfs tensor was also found by HFEPR: $E = 0.009$ cm^{-1}, since the agreement between experiment and simulation was much worse if E was assumed to be zero. The g-matrix values are very close to 2.00, with $g_{\perp} = 1.995$ and $g_{\parallel} = 2.000$.

The **[CoCo]** and **[CoNi]** complexes gave no HFEPR signals over the entire magnetic field range, despite use of multiple frequencies. The **[CoFe]** complex is very air-sensitive, and the sample handling/loading procedures for HFEPR inevitably led to formation of a modest amount (qualitatively, based on other studies) of an unknown decomposition product with $S = 1/2$, which was easily seen by HFEPR, but no signals were attributable to the $S_{total} = 3$ ground state found by magnetometry measurements.

EPR simulations using the spin-Hamiltonian parameters obtained by magnetometry for **[CoCo]**, **[CoNi]**, and **[CoFe]** indicate that a wealth of HFEPR signals should in principle be observed for these integer spin complexes at the microwave frequencies available to us. The question then arises as to why no such signals were observed, although the **[CoMn]** complex was fully amenable to study by HFEPR.

A qualitative reason for this difference is attributed to the nature of the M single ions in **[CoM]** complexes. For M = Mn(II), the single ion has an orbitally spherically symmetric, half-integer spin electronic ground state ($^6A_1$ in T_d) and generally smaller zfs and longer electron spin relaxation times, so that conventional EPR spectra are readily observed for Mn(II).[50] However, for the other M single ions, there are significant orbital contributions to the ground state, resulting in larger zfs and faster electronic relaxation times. For both Fe(II) and Ni(II), the electronic ground states are orbitally degenerate and with integer spin, in T_d symmetry, respectively ^5E and $^3T_1$, and both are fraught with severe difficulties in observation of conventional EPR spectra. For Co(II), the ground state is orbitally nondegenerate and with half-integer spin, $^4A_2$ in T_d, but zfs can be quite significant for Co(II), and observation of conventional EPR can be problematic.[51]

These effects that are manifest in the EPR behavior of the Fe(II), Ni(II), and Co(II) single ions are likely carried over into the molecular square complexes, where there is the added complication that magnetic exchange interactions lead to complicated "ladders" of spin states, providing further, efficient relaxation pathways. For example, a calculation of energy levels for a four-spin system with $S_1 = S_3 = 1/2$ with $g = 2.10$ (i.e., Co(triphos)) and with $S_2 = S_4 = 1$ with $g = 2.20$ and $D = -10$ cm^{-1} (reasonable for Ni(II)) and $J_{12} = J_{34} = -10$ cm^{-1} (all other $J_{ij} = 0$) gives 36 spin states in six levels (either 4- or 8-fold degenerate in the zero field), each separated from the next highest levels by ~ 3–5

(48) Krzystek, J.; Zvyagin, S. A.; Ozarowski, A.; Trofimenko, S.; Telser, J. *J. Magn. Reson.* **2006**, *178*, 174–183.
(49) Krzystek, J.; Park, J.-H.; Meisel, M. W.; Hitchman, M. A.; Stratemeier, H.; Brunel, L.-C.; Telser, J. *Inorg. Chem.* **2002**, *41*, 4478–4487.
(50) Drago, R. S. *Physical Methods in Chemistry*; Saunders: Philadelphia, 1992; Chapter 13.
(51) Krzystek, J.; Zvyagin, S. A.; Ozarowski, A.; Fiedler, A. T.; Brunold, T. C.; Telser, J. *J. Am. Chem. Soc.* **2004**, *126*, 2148–2155.
(52) Boudreaux, E. A.; Mulay, L. N. *Theory and Application of Molecular Paramagnetism*; Wiley: New York, 1976.

cm^{-1}. Such a system is not conducive to long electronic spin relaxation times, which would lead to homogeneous broadening of EPR transitions, necessitating a low temperature for their observation. Low temperatures were employed, yet no signals were observed. We thus suspect that, for the **[CoNi]**, **[CoFe]**, and **[CoCo]** molecular square complexes, in addition to faster electronic relaxation than in **[CoMn]**, which leads to homogeneous broadening of EPR lines, there is a distribution of molecular conformations, not manifest by the thermal parameters in the X-ray crystal structures. If present, such small structural irregularities would lead to a distribution of spin Hamiltonian parameters ("*D*-strain" and "*g*-strain") and severe inhomogeneous broadening, with the result that EPR transitions are broadened beyond observation.

Conclusions

This work represents the first time that a paramagnetic metal center with a square-pyramidal geometry has been introduced into a molecular square motif. The successful building block for assembly of these molecular squares is $Co(triphos)(CN)_2$, which contains a square-pyramidal low-spin ($S = 1/2$) Co(II) ion. Five complexes of the general formula $\{[Co(triphos)(CN)_2]_2[MCl_2]_2\}$ (M = Mn, Fe, Co, Ni, Zn; abbreviated as **[CoM]**) were prepared by reaction of $Co(triphos)(CN)_2$ with the corresponding MCl_2 compound (or $Fe_4Cl_8(THF)_6$). These **[CoM]** complexes can be described as molecular squares in which the square-pyramidal Co(II) ions are linked by tetrahedral M(II) ions. Magnetic and EPR measurements of the **[CoZn]** complex ($S_{Zn} = 0$) supported the conclusion that there is no magnetic interaction between the low-spin Co(II) ions. However, in the case of paramagnetic M(II) centers, there is significant antiferromagnetic coupling between the Co(II) and M(II) ions. This interaction generally follows the spin-coupling model: $S_{total} = S_{M1} - S_{Co1} + S_{M2} - S_{Co2} = 2S_M - 1$. Thus, for **[CoMn]**, $S_{total} = 4$; for **[CoFe]**, $S_{total} = 3$; for **[CoCo]**, $S_{total} = 2$; for **[CoNi]**, $S_{total} = 1$.

An important outcome of this study is that the building-block approach yields a family of cyanide clusters with a predicted geometry. These results hold promise for the area of molecular magnetism because, in addition to the single-ion anisotropy, cluster geometry is a major factor that produces shape anisotropy. A square geometry is one of the most desirable shapes to increase shape anisotropy because of its planarity. By taking advantage of this geometry, we have achieved the preparation of high-spin clusters, which have appreciable *D* values, as determined by magnetometry and, in the case of **[CoMn]**, by HFEPR measurements. Moreover, these square compounds have negative *D* values, which increase the interest in this family of compounds, since a negative *D* value is a prerequisite for single-molecule and single-chain magnetism. In considering the applications for these compounds, it is important to note that the **[CoM]** clusters could be used to prepare larger assemblies and extended clusters. Despite the presence of the bulky triphos ligands, space-filling diagrams of the squares (Figure 2) clearly indicate that the chloride ligands of the tetrahedral M(II) ions could be replaced by bridging ligands for the purpose of linking the squares into higher-nuclearity molecule-based architectures.

Acknowledgment. This research was supported by NSF (PI grant CHE-0610019), in part, DOE (DE-FG03-02ER45999) and the Robert A. Welch Foundation (KRD). Funding of the CCD diffractometer (CHE-9807975) at Texas A&M University and the SQUID magnetometer (NSF 9974899) by NSF is also gratefully acknowledged. EPR studies were supported by the National High Magnetic Field Laboratory, which is funded by NSF through Cooperative Agreement DMR 0084173, the State of Florida, and the DOE. The 25-T resistive magnet was funded by the W. M. Keck Foundation.

Supporting Information Available: Plots of *M* vs *H*/*T* for the various study compounds, X-band and V-band spectra of $Co(triphos)(CN)_2$, and CIF files for the various study compounds. This material is available free of charge via the Internet at http://pubs.acs.org.

IC702084E